

A model for predicting lateral buckling in rails

D. H. Allen

Texas A&M University, College Station, TX, U.S.A.

G. T. Fry

TTCI, Pueblo, CO, U.S.A.

ABSTRACT: This paper presents a computational model for predicting lateral buckling of rail structures subjected to long-term cyclic thermomechanical loading. Emphasis is placed on a tool that is both simple to deploy and accurate for environmental circumstances normally encountered by rail structures subjected to a wide range of loading conditions. Special emphasis is given to ability of the model to predict the effects of both temperature change and long-term degradation of track structure properties such as crosstie-ballast interface friction. The model is briefly described herein, and example problems are presented demonstrating the power of the resulting algorithm for use by railway engineers in the field.

1 INTRODUCTION

Lateral buckling of rails is a rather complicated phenomenon that is observed in a wide variety of physical circumstances. It often occurs instantaneously with little or no warning. According to the United States Federal Railroad Administration (FRA 2015), approximately 10% of all rail incidents within the U.S. are related to rail buckling (see Fig. 1).

TTCI and the Center for Railway Research at Texas A&M University have teamed up to develop a predictive methodology that is capable of accurately predicting the onset of rail buckling.



Fig. 1 Photograph Showing a Local Railway Buckle

2 MODEL DEVELOPMENT

When rails are butt welded they are unable to undergo significant extension in the longitudinal direction, thereby sometimes resulting in lateral deformations as a means of relieving strain energy built up within the rails by longitudinal track loads. These longitudinal loads can be applied to the rail by trains, but they also occur due to thermal strains that result when the local temperature is higher than the so-called rail-neutral temperature (the temperature at which there are no thermally induced longitudinal loads within the rail). For this reason, buckling of rails is oftentimes observed to occur on a hot summer day, thereby leading to the term “thermal buckling” of rails.

However, this is an oversimplification of the physical phenomenon of rail buckling. There are actually several factors that contribute to rail buckling, not the least of which is the slow deterioration of the track structure over time. The primary issue here is the long-term degradation of the longitudinal and lateral coefficients of friction of the interface between the track structure and the underlying ballast. As trains apply increasing tonnage to the track structure, lateral load-carrying capability of this interface slowly decreases due to both grinding and settling resulting from slippage during train passage. Secondary causes include the rotational stiffness applied to the rail by crosstie connectors and settling of the ballast.

Because the track displaces laterally during buckling, the lateral coefficient of friction is a key contributor to track buckling. As shown in Fig. 2, Single-tie push tests (STPT) have demonstrated that this coefficient of friction is highly nonlinear (Read et al 2011). In fact, previous research has shown that rail temperature, rail-ballast interface friction, and the rail-crosstie structural configuration must be included within any rail buckling model in order to accurately predict rail buckling (Kerr 1978, Tvergaard and Needleman 1981, Grissom and Kerr 2006). The authors are therefore focusing on these effects in their attempts to model lateral track buckling. Specifically, the following physical effects are included within the model currently under development (Allen and Fry, 2016a): 1) temperature of the rail; 2) geometric nonlinearities due to large deformations; 3) nonlinear and degrading friction between the track structure and ballast; and 4) rotational stiffness of the crosstie connectors.

Unfortunately, accounting for all of these contributing factors necessarily results in a mathematical model that cannot be solved analytically. Accordingly, the authors have developed a self-contained computational algorithm for predicting lateral buckling in rails (Allen and Fry 2016b) that is based on large deformation Euler-Bernoulli beam theory (Euler 1744, Allen and Haisler 1985) cast within the finite element method (Reddy 1984) (see Fig. 3). Nonlinearity in the algorithm results from large deformations in the rail in the deformed configuration, finite strains, and nonlinearities in the friction between the crossties and ballast. This nonlinearity is accounted for using Newton iteration.

We present here a brief summary of the model development. Accordingly, consider a section of track structure, as depicted in Fig. 3. When viewed in the horizontal plane, a typical rail with mechanical and thermal loading is shown in Fig. 4.

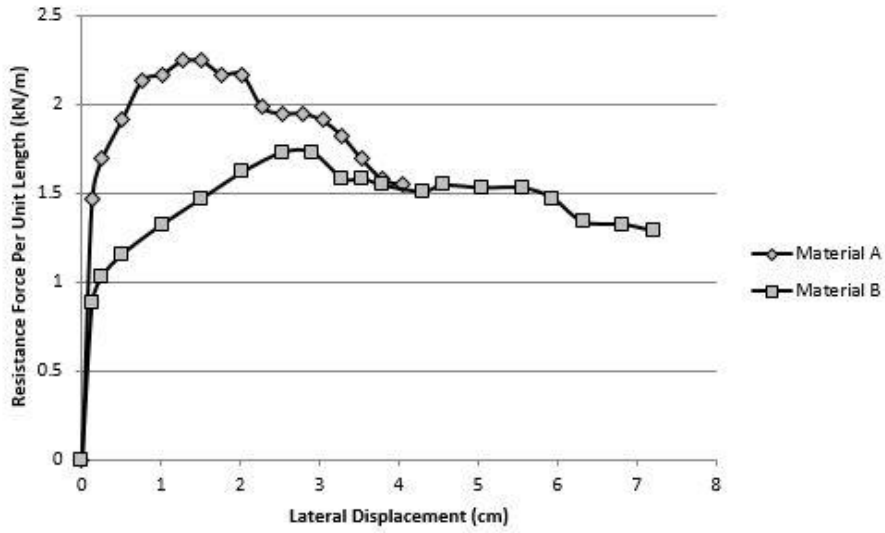


Fig. 2 Typical Lateral Load vs. Displacement from Single Tie Push Tests (STPT) (Read et al 2011)

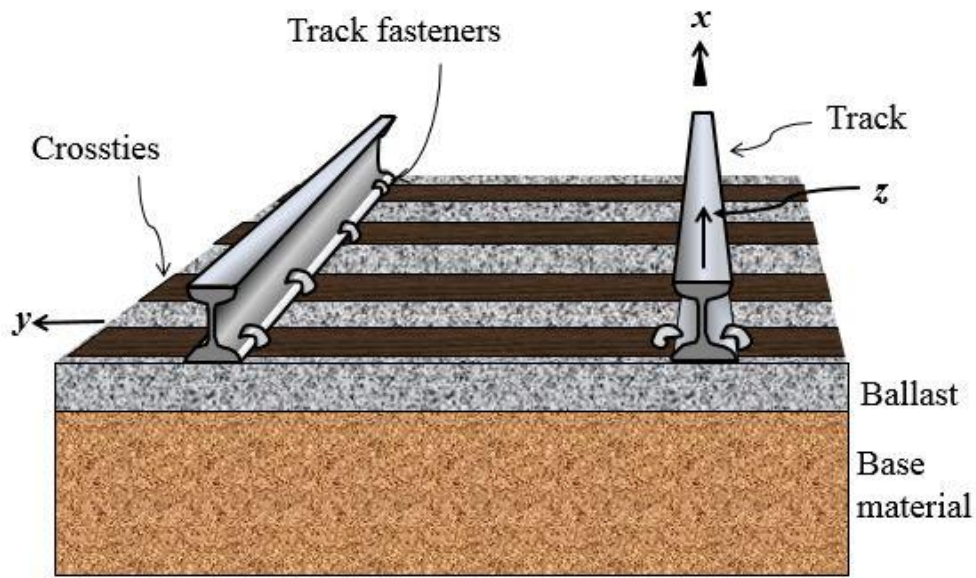


Fig. 3 Generic Rail with Right-Handed Coordinate System as Shown

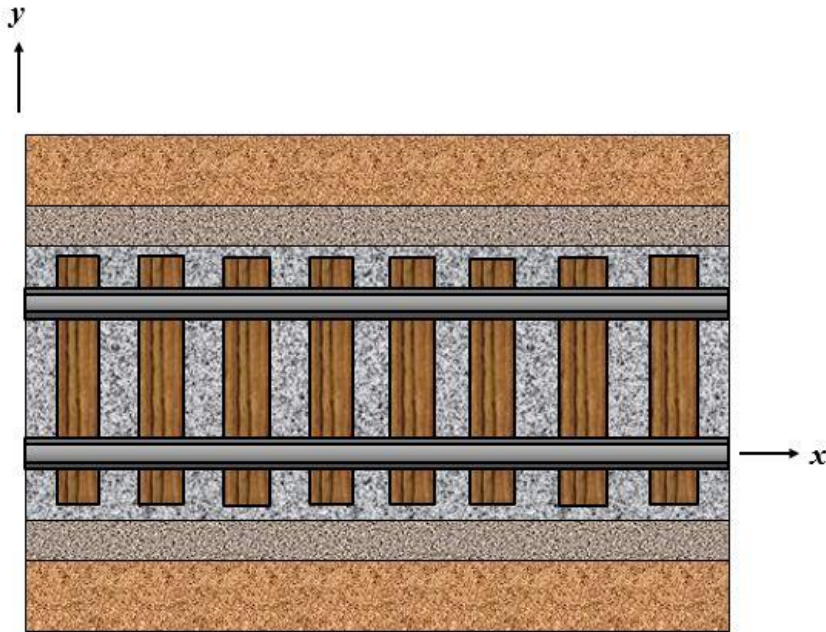


Fig. 4 Horizontal View of Typical Rail Loaded Mechanically and Thermally

In order to construct a model for thermal buckling of the track structure, it is assumed that the structure may be adequately modeled as an Euler-Bernoulli beam-column (Euler 1744, Allen and Haisler 1985, Grissom and Kerr 2006). Furthermore, whereas Lim and coworkers (Lim et al 2003) have shown that the out-of-plane deformation component, $w=w(x)$, may be significant, it will be assumed herein that this component of deformation may be neglected. Using these two assumptions, the track structure shown in Figs. 3 and 4 may be idealized as a single slender beam, as shown in Fig. 5. As shown in the figure, the centroidal axis of the rail may deform in the two horizontal coordinate directions, and the components of this displacement are denoted by $u(x, t)$ and $v(x, t)$, respectively. Similarly, the components of stress $\sigma_{xx}(x, y, t)$ and $\sigma_{yy}(x, y, t)$ are shown on an arbitrary cross-section of the rail in Fig. 6.

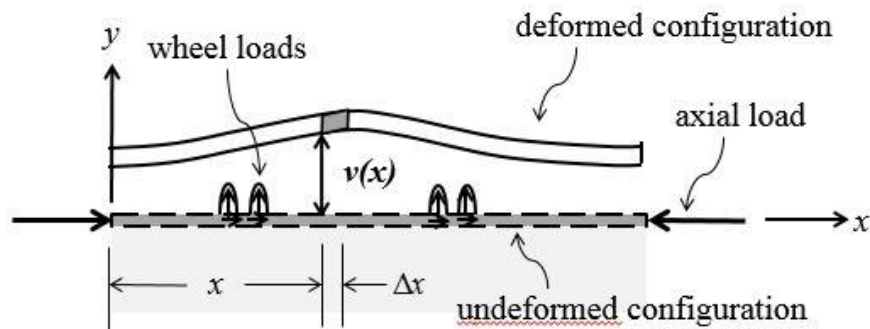


Fig. 5 Top View of the Rail Showing Horizontal Transverse Displacement Component in the Deformed Configuration

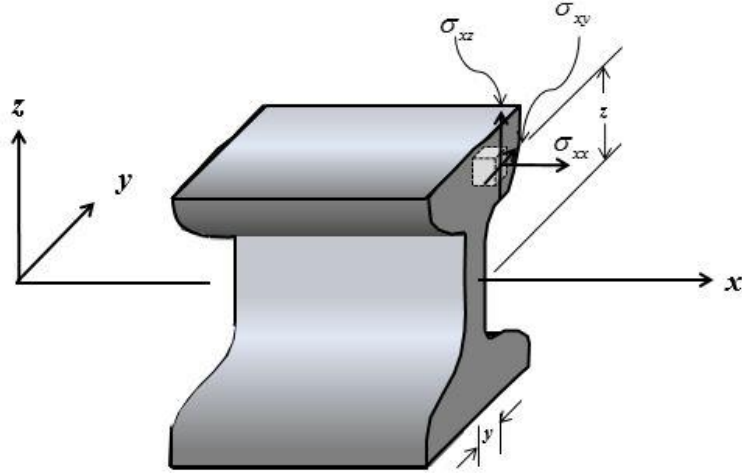


Fig. 6 Components of Stress on an Arbitrary Cross-Section of the Rail

The load per unit length applied to the centroidal axis of the rail is composed of components $p_x(x, t)$ and $p_y(x, t)$ in the x and y coordinate directions, respectively. In addition, the normal component of force per unit length applied to the bottom of the rail due to the normal displacement component $v(x, t)$ is denoted as $-k_y v(x, t)$, where $k_y(x, t)$ is the lateral coefficient of friction and the negative sign is employed so that the base stiffness is non-negative when the resultant is positive due to lateral displacement of the rail. Similarly, the axial component of force per unit length applied to the bottom of the rail due to the axial component of displacement $u(x, t)$ is denoted $-k_x u(x, t)$, where $k_x(x, t)$ is the axial coefficient of friction.

Note also that the stress distribution on the two vertical cuts within the rail are denoted generically by the two infinitesimal stress elements on these faces. Consistent with Euler-Bernoulli beam theory the force and moment resultants in the x - y plane are now defined as follows (Allen and Haisler 1985):

$$P = P(x, t) \equiv \int_A \sigma_{xx} dA \quad (1)$$

$$V_y = V_y(x, t) \equiv \int_A \sigma_{xy} dA \quad (2)$$

$$M_z = M_z(x, t) \equiv -\int_A \sigma_{xx} y dA \quad (3)$$

where A is the cross-sectional area of the rail, and y is the horizontal distance from the centroid of the rail. The above resultants may now be utilized to construct the free body diagram shown in Fig. 7. Note that the rotational resistance per unit length, $r_z(x, t)$, has been included in the free body diagram. This resistance, due to the crosstie and fastener resistance to the rotation of the track, was previously introduced by Grissom and Kerr (Grissom and Kerr 2006). The inclusion of this term is explained by the fact that since the ballast and fasteners impede rigid-body rotation of the crossties with the track, the crossties apply a moment in the opposite direction from the rotation of the track about the z -axis, and this moment is applied to the rail by the fastener connections.

These moments are therefore pointwise in nature, but are depicted as distributed moments per unit length, $r_z(x, t)$, as a simplification of the model.

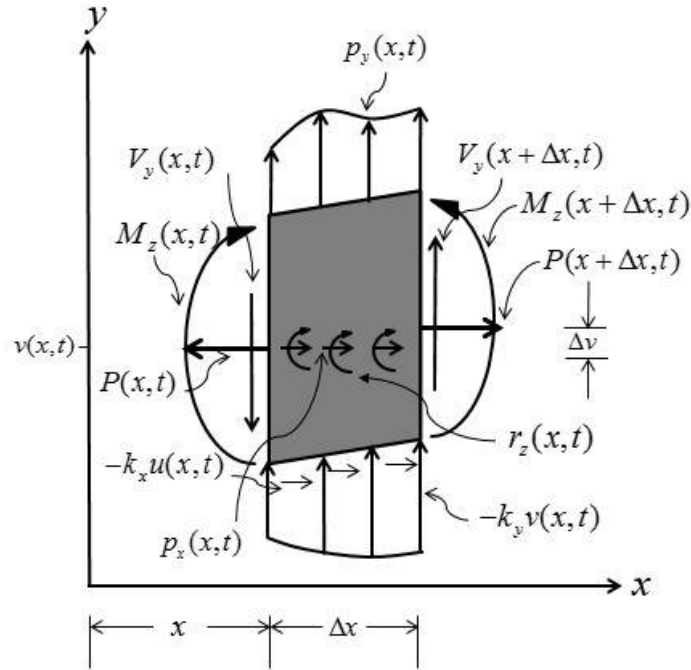


Fig. 7 Resultant Forces and Moments Applied to a Differential Element of the Rail

This rather ingenious aspect of the model has the advantage that it captures the physical effect of the crossies on the rail response without actually requiring the crossies to be included as structural members, a complicating factor included in at least one more complex model (Lim et al 2003). Finally, note that the differential element of the rail shown in Fig. 6 is depicted in the deformed configuration, so that the axial force affects the transverse displacement of the rail. This necessarily causes the response of the rail to be geometrically nonlinear.

Assuming linear thermoelastic behavior, the axial stress within the rail is given by the following constitutive equation:

$$\sigma_{xx} = E(\varepsilon_{xx} - \alpha\Delta T) \quad (4)$$

Where E is the modulus of elasticity of the rail, ε_{xx} is the axial strain within the rail, α is the coefficient of thermal expansion within the rail, and ΔT is the temperature change from the rail neutral temperature, which is assumed to be temporally variable, but spatially constant and known a priori in the current paper. Furthermore, the axial strain is approximated by (Tvergaard and Needleman 1981, Grissom and Kerr 2006):

$$\varepsilon_{xx} = \frac{du}{dx} + \frac{1}{2}\left(\frac{dv}{dx}\right)^2 \quad (5)$$

In addition, it is assumed that the relation between the rotational stiffness and the track rotation is given by the following constitutive relation:

$$r_z = -S\theta \quad (6)$$

Note that in the above equation it is assumed that the relation between rotation of the track structure about the z coordinate axis and the angle of rotation is linear (Grissom and Kerr 2006). Whereas limited experimental data support this assumption (Grissom and Kerr 2006), it is to be noted that the rotational stiffness, S , depends strongly on the type of fasteners used (Grissom and Kerr 2006).

Furthermore, in the current research it is assumed that S depends not only on the type of fasteners connecting the track to the cross-ties, but that it is also a weak function of the number of cycles of loading, n_c , previously applied to the track structure. Thus, at any point in time the relationship described by equation (6) is assumed to apply, but the value of S is at that point in time a constant depending on both the type of fasteners deployed and n_c , thereby quasi-linearizing this effect on the rail response. This assumption is based on anecdotal observations suggesting that ballast settlement, grinding, spallation and rearrangement over time can affect the rotational resistance of the cross-tie-fastener system to track rotation, and such an assumption will be validated experimentally in future research.

Independent Variables: x, t

Known Inputs:

Loads: $p_x = p_x(x, t), p_y = p_y(x, t), 0 < x < l$

Temperature change: $\Delta T = \Delta T(t) = \text{known}$

Geometry: A, I_{zz}

Material Properties: α, E, k_x, k_y, S

Unknowns: $u, v, \sigma_{xx}, P, V_y, M_z = 6 \text{ unknowns}$

Field Equations:

	No. of Equations
(7) $\frac{dP}{dx} = -p_x + k_x u$	1
(8) $\frac{dV_y}{dx} = k_y v - p_y$	1
(9) $\frac{dM_z}{dx} = -V_y - (S - P) \frac{dv}{dx}$	1
(10) $\sigma_{xx} = \frac{(P + P^T)}{A} - \frac{M_z}{I_{zz}} y - E\alpha\Delta T$	1
(11) $\frac{du}{dx} = \frac{(P + P^T)}{EA} - \frac{1}{2} \left(\frac{dv}{dx} \right)^2$	1
(12) $\frac{d^2v}{dx^2} = \frac{M_z}{EI_{zz}}$	1

Table 1 Model for Predicting the Rail Response

Applying Newton’s first law to the forces in the x coordinate direction and moments about the z axis in Fig. 6 together with equations (1)-(6) will result in the general two dimensional formulation shown in Table 1 for a generic rail subjected to mechanical and spatially constant thermal loading (Kerr 1974, 1978, Allen and Haisler 1985, Allen and Fry, 2016a), where it should be noted that:

A is twice the cross-sectional area of the rail

I_{zz} is twice the moment of inertia of the rail about the z centroidal axis

$P^T = EA\alpha\Delta T$ is the axial load induced by temperature change

It should be apparent that the problem formulated in Table 1 represents a well-posed boundary value problem when appropriate boundary conditions are imposed. However, as there are 6 coupled equations in 6 unknowns, it may be exceedingly difficult to solve, depending on the loading conditions and the material properties involved. In particular, the friction coefficients k_x and k_y are observed to be highly nonlinear. Accordingly, although at least one solution has in fact been obtained for specialized conditions (Grissom and Kerr 2006), closed form solutions are difficult to obtain for this problem.

Alternatively, computational solutions are possible using the finite element method, and this approach has been employed by the authors to construct a self-contained finite element algorithm (Allen and Fry, 2016b). Although space does not allow for a detailed reconstruction of the formulation here, the procedure for constructing a finite element model of the rail structure is as follows (Reddy 2015):

- 1) Construct a variational form of the equations given in Table 1;
- 2) Discretize the resulting variational form using cubic beam elements;
- 3) Include all nonlinearities in the formulation;
- 4) Account for nonlinearity using Newton iteration; and
- 5) Model the progression of lateral deformations in the rail using a time-stepping procedure.

The model has been validated against a number of simplified problems for which analytic solutions exist (Allen and Fry 2016b). An example of this validation is shown in Fig. 8. These validation problems have confirmed the accuracy of the finite element formulation.

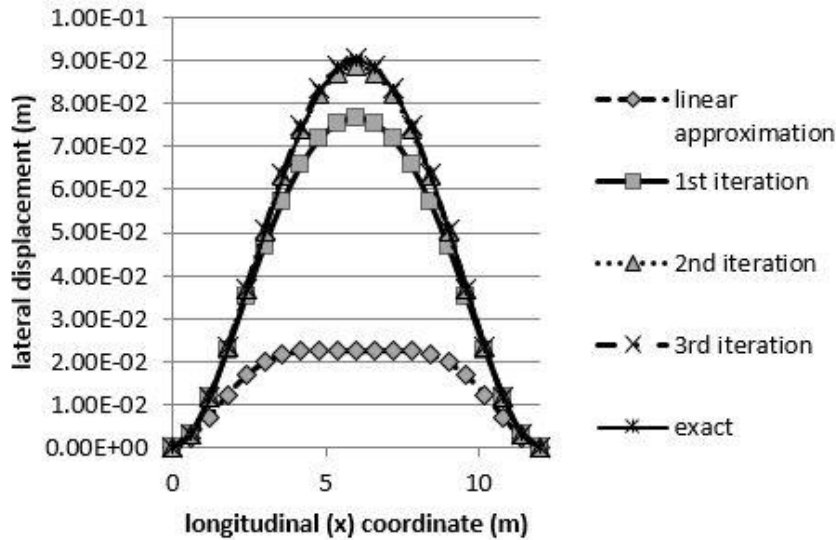


Fig. 8 Comparison of Finite Element Approximations for Each Iteration (20 element mesh) to Exact Solution for A Typical Nonlinear Example Problem

3 MODEL PREDICTIONS

The resulting computational algorithm is self-contained and can be deployed on a laptop computer, so that readily available track-structure information can be utilized to predict local track buckling a priori. Specifically, the following information is necessary in order to deploy the algorithm:

- track-structure geometric configuration, including residual lateral deformations
- previously applied track tonnage
- current and rail-neutral track temperature
- both cross-tie and track-cross-tie connection type
- current nonlinear coefficients of longitudinal and lateral friction (as functions of track tonnage)

Typical results obtained with the model are shown in Fig. 9, wherein critical temperature change necessary to induce buckling is plotted against buckle length for a variety of (constant) coefficients of friction, k_z , between cross-ties and ballast for a typical track structure (Allen and Fry 2016a).

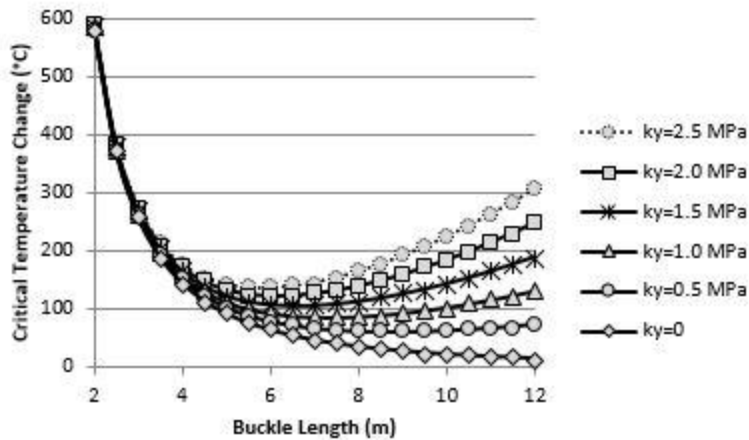


Fig. 9 Predicted Critical Temperature Change for Rail Buckling as a Function of Buckle Length for Several Different Friction Coefficients

A significant feature of the model is the ability to account for the degradation of material properties within the rail structure due to cyclic loading and environmental conditions. Toward this end, the authors have developed a model for predicting the nonlinear coefficients of friction. For example, the nonlinear coefficient of lateral friction is input by curve fitting to available experimental data. A power law is used toward this end, with a typical fit for Material B in Fig. 2 shown in Fig. 9.

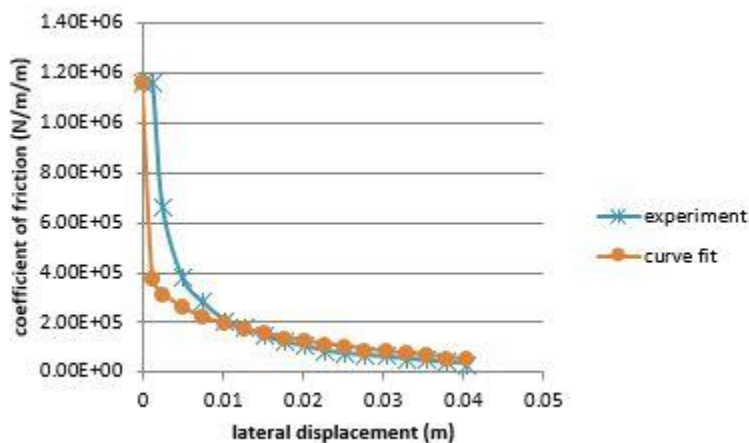


Fig. 10 Curve Fit of Coefficient of Lateral Friction Used in the Algorithm to Material B Shown in Fig. 2

The friction model has also been extended to account for cyclic loading, as shown in Fig. 11. Unfortunately, experiments have not been performed in the field to determine how this property degrades over time in track structures. Therefore, one requirement for future deployment of the model within the field is that railway engineers will necessarily be required to perform field tests (such as the STPT test) over the life of the rail structure (or equivalently, as a function of tonnage), thereby providing material coefficients necessary to deploy the track structure algorithm.

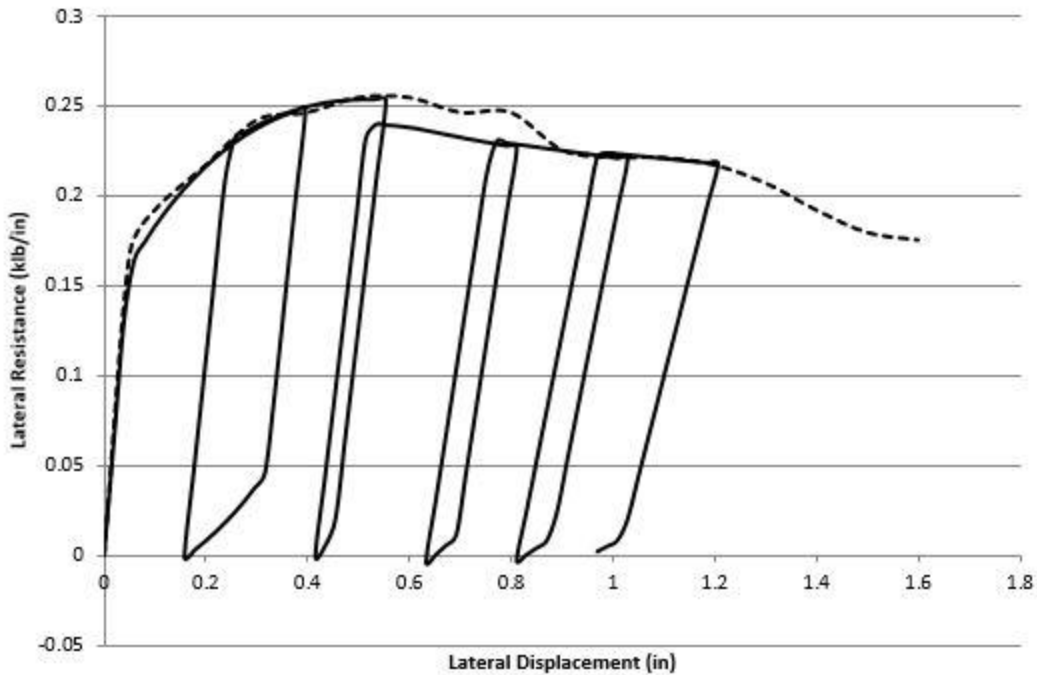


Fig. 11 Comparison of Cyclic Friction Model (bold line) to monotonic experiment (dotted line, also Material A in Fig. 2)

4 CONCLUSIONS

The authors have focused on two innovations in an attempt to both improve accuracy of rail buckling models and provide a tool that is convenient for deployment by field engineers. It is hoped that improved accuracy will be achieved with the inclusion of the nonlinear and tonnage history friction model described herein. The development of a self-contained finite element algorithm is intended to provide a convenient tool for deployment in the field.

Because this new algorithm is self-contained, it can be deployed without recourse to (often expensive) commercial software. Furthermore, the algorithm can be easily interfaced with data gathering devices such as machine vision currently under development at TTCI, so that local environmental conditions, residual deformations in the track, track structural configuration, and track structure-ballast interface friction properties can be input to the algorithm “on the fly”, thereby providing railway engineers valuable information for deciding when and where intervention is required in order to avoid rail incidents induced by buckling.

5 ACKNOWLEDGMENTS

The authors acknowledge the support provided for this research by TTCI.

6 REFERENCES

Allen, D.H. and Haisler, W.E. 1985. Introduction to aerospace structural analysis, Wiley.

Allen, D.H. and Fry, G.T. 2016a. Analysis of a rail subjected to mechanical and thermal loading, CRR Report No. 2016-01, Texas A&M University.

Allen, D.H. and Fry, G.T. 2016b. Finite element formulation for thermal buckling of rails, CRR Report No. 2016-02, Texas A&M University.

Allen, D.H., Fry, G.T. and Davis, D. 2016. Development of a model for describing nonlinear lateral resistance of track ballast, Technology Digest, TD-16-029.

Euler, L. 1744. Method inveniendi lineas curvas, Opera Omni, St. Petersburg, Russia.

Grissom, G. and Kerr, A. 2006. Analysis of lateral track buckling using new frame-type equations, Int J Mech Sci, 48:21-32.

Kerr, A. 1978. Analysis of thermal track buckling in the lateral plane, Acta Mechanica, 30:17-50.

N Lim, N Park and Y Kang (2003) Stability of continuous welded track, Computers & Structures, 81:2219-2236

Railroad Accident Statistics 2015. Federal Railroad Administration, downloaded at:<http://safetydata.fra.dot.gov/officeofsafety/publicsite/Query/TrainAccidentsFYCYWithRates.aspx>

D Read, R Thompson, D Clark and E Gehringer (2011) Results of Union Pacific concrete tie track panel shift tests, Technology Digest, TD-11-004

Reddy, J.N. 1984. An introduction to the finite element method, McGraw-Hill.

Reddy, J.N. 2015. An introduction to nonlinear finite element analysis (second edition), Oxford.

Tvergaard, V. and Needleman, A. 1981. On localized thermal track buckling, Int J Mech Sci, 23:577-587.